Origin of tunnel electroresistance effect in $PbTiO_3$-based multiferroic tunnel junctions

Andy Quindeau,[1,*] Vladislav Borisov,[2,3] Ignasi Fina,[1,4] Sergey Ostanin,[1] Eckhard Pippel,[1] Ingrid Mertig,[1,3] Dietrich Hesse,[1] and Marin Alexe[4]

[1]*Max Planck Institute of Microstructure Physics, Weinberg 2, D-06120 Halle, Germany*
[2]*Goethe University Frankfurt, Senckenberganlage 31, D-60325 Frankfurt am Main, Germany*
[3]*Institute of Physics, Martin Luther University Halle-Wittenberg, D-06099 Halle, Germany*
[4]*Department of Physics, University of Warwick, Coventry CV4 7AL, United Kingdom*

(Received 20 February 2015; revised manuscript received 15 May 2015; published 16 July 2015)

The mechanism of the tunnel electroresistance effect of a $Co/PbTiO_3/La_{0.7}Sr_{0.3}MnO_3$ multiferroic tunnel junction is studied in detail using experimental and theoretical methods. Based on experimental data, we present a model that explains the correlation between the polarization of the ferroelectric material and the observed resistance state based on the effective change of the tunnel barrier thickness. We show that the observed thickness variation can neither be completely attributed to the asymmetric inverse piezoelectric effect in the classical sense, nor to asymmetric screening of the polarization charge. The analysis of detailed *ab initio* calculations quantitatively demonstrates that a mixture of electronic and structural phenomena is responsible for the change in effective tunnel barrier thickness upon polarization reversal. On the one hand, the ferroelectric material exhibits a reversible metallization at one of the interfaces, which shifts the boundary between the ferroelectric material and the electrode. On the other hand, a piezoelectric effect that stems from different terminations of the ferroelectric ultrathin film towards the electrodes magnifies this effect. Combined, the electrically switchable effective change in thickness is as large as 0.15 nm, which dominates the resistive switching effect in the presented junction that involves a 3.2 nm thin $PbTiO_3$ film. This work contributes to the deeper understanding of fundamental mechanisms that lead to tunnel electroresistance and imposes new ways for tailoring the characteristics of electroresistive tunnel junctions.

DOI: 10.1103/PhysRevB.92.035130 PACS number(s): 73.40.Gk, 77.55.fg

I. INTRODUCTION

Tunnel electroresistance (TER) is the reversible switching of the tunnel conductance through an ultrathin ferroelectric (FE) film, confined between two conducting electrodes in simple capacitor geometry. By applying an electric field, a tunnel current occurs, which is modulated by the direction of ferroelectric polarization of the barrier. If the applied electric field is larger than the ferroelectric coercive field of the ultrathin FE tunnel barrier, the junction switches either into a fully saturated [1,2] or semianalogous [3,4] FE domain configuration, which can be used for digital or memristive [5] logic operations. One of the benefits of FE tunnel junctions (FTJ) is the low energy consumption per switching, which scales with the junction capacitor area and is only limited by the theoretical minima described by Landau theory.

Since the prediction [6–8] and discovery [1,2,9] of the tunneling electroresistance in FTJ, the TER effect is often ascribed to the polarization-induced electronic reconstruction at asymmetric ferroelectric/metal (FE/M) interfaces [8,9] that lead to TER ratios of up to 10 000 [10,11]. Another suggested mechanism is the thickness variation of ferroelectrics [7], which had originally been conceived as being a direct result from piezoelectric deformation of the ferroelectric barrier [12] and is different for the two polarization orientations.

The actual resistance relation of the TER with respect to the FE polarization direction is still under discussion, as is evidenced by the large discrepancy between the found TER sign in different works. In experiments on $BaTiO_3/SrRuO_3$ for example, where the tunnel current through a FE layer was measured via a conductive-AFM (c-AFM) tip, the explanation given by Zhuravlev *et al.* [6] was used to describe TER [1,2]. This led to high resistance states for FE polarization pointing towards the material with the lower screening length (in this case the AFM tip). In other experiments, the high resistance states were obtained for FE polarization pointing exactly into the opposite direction, respectively, towards the material with larger screening length. In these cases the reasoning was much less thoroughly discussed [9,13].

Jang *et al.* have recently addressed this issue by considering the influence of hole doping concentrations in $(La_{0.7}Sr_{0.3})MnO_3$ [14]. The results suggested that hole accumulation and depletion in the $(La_{0.7}Sr_{0.3})MnO_3$ bottom electrode could play the central role for tunnel junctions with $Pb(Zr_{0.2}Ti_{0.8})O_3/(La_{0.7}Sr_{0.3})MnO_3$ composition. However, the investigated $(La_{0.7}Sr_{0.3})MnO_3$ bottom electrodes with only 5 nm thickness were close to the regime where field effects induced by $Pb(Zr_{0.2}Ti_{0.8})O_3$ yield a strong change in transport properties upon FE polarization reversal and thus the conclusions drawn still lag unambiguity.

Separation of the coexisting contributions in TER effects is one of the challenges addressed in this work. An improved understanding of the fundamental mechanisms could be used to enhance the resistance ratio (OFF/ON) and associated (magnetoelectric) effects via interface engineering. Here, we present our study on a $PbTiO_3$-based tunnel junction with focus on the origin of the observed TER effect. Conjointly with *ab initio* calculations, detailed analysis of transport data will eventually be the basis for a model, which explains the found TER based on an interface phenomenon occurring on the atomic scale.

*Corresponding author: quindeau@mpi-halle.de

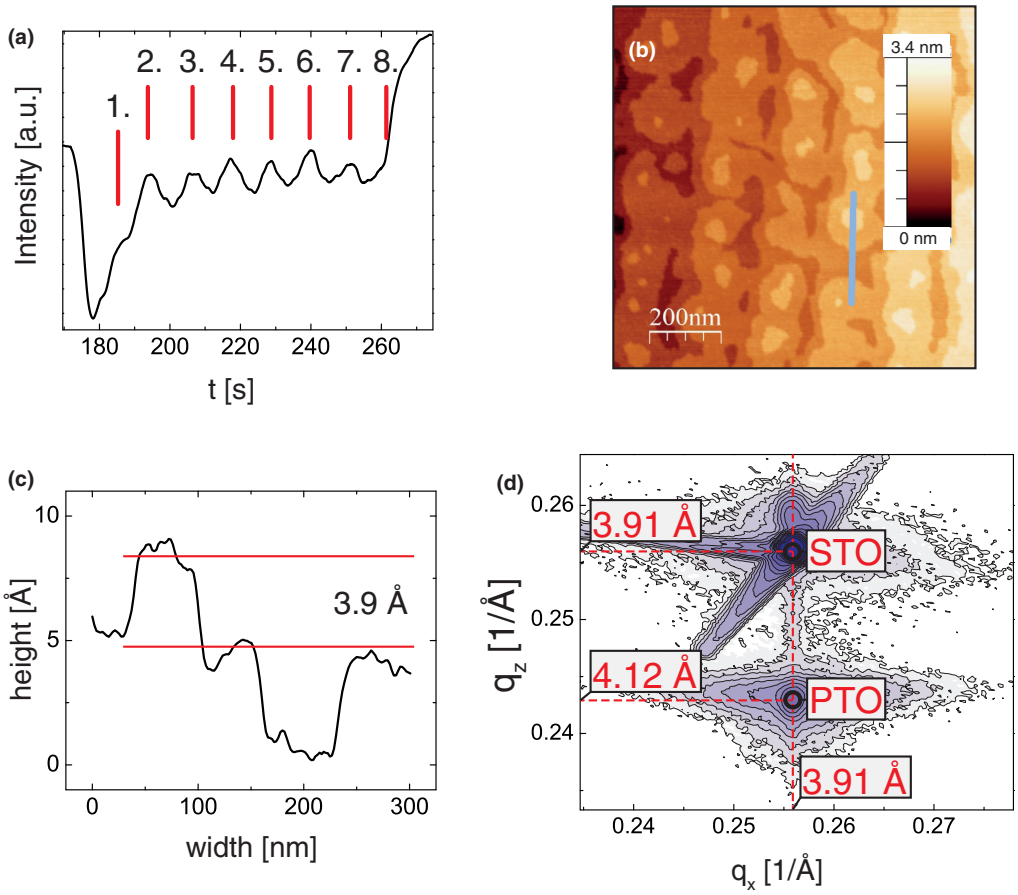

FIG. 1. (Color online) *Characteristics of the ultrathin film* $PbTiO_3$. (a) RHEED main reflection intensity oscillations during growth. At the eighth maximum (corresponding to a thickness of around 3.2 nm), the deposition was stopped. (b) AFM image of the film after deposition. The steps are atomically flat and resemble the step height of the underlying $SrTiO_3$ substrate. (c) Line profile of the AFM topography in (b). (d) XRD reciprocal space map of the PTO/LSMO heterostructure, showing fully strained PTO and LSMO films.

II. METHODOLOGY

To study the characteristics of tunnel junctions, clean interfaces between the FE and metallic electrodes are crucial to avoid transport through defects or pin-hole conduction [15,16]. Therefore, atomically flat films were grown epitaxially via reflection high-energy electron diffraction (RHEED) -controlled pulsed laser deposition on (001) $SrTiO_3$ substrates. As a bottom electrode we chose $(La_{0.7}Sr_{0.3})MnO_3$ (LSMO), which was grown using a laser fluence of 1 J/cm^2, repetition rate of 1 Hz, 600 °C substrate temperature, and an oxygen pressure of 0.15 mbar. RHEED oscillations and patterns during the LSMO deposition suggest layer-by-layer growth and smooth two-dimensional surface morphology. $PbTiO_3$ (PTO) deposition was performed *in situ* at an increased oxygen pressure of 0.28 mbar using a laser fluence of 0.4 J/cm^2 and 4 Hz repetition rate. The good quality of PTO is revealed by the presence of clear RHEED oscillations [Fig. 1(a)] and the morphology of the film [Fig. 1(b)]. An 80-nm thick cobalt top electrode was deposited by sputtering followed by a 2 nm gold passivation layer, deposited via thermal evaporation. The sample was then structured by a standard lithography and wet etching process using a potassium iodide based etchant to produce capacitors of 1600 μm^2 area.

The x-ray diffraction (XRD) reciprocal space map in Fig. 1(d) shows that the structure is fully strained in respect to $SrTiO_3$ (001). Transmission electron microscopy (TEM) investigations (Fig. 2) not only confirm the thickness of the ferroelectric to be 3.2 nm, but also demonstrate the high quality of the layers and interfaces. A previous detailed analysis on similar films shows that direct tunneling is expected for ferroelectric films with thickness below 4 nm [17]. It can be seen on the images in Fig. 2; even the cobalt top electrode possesses features of textured growth.

Transport measurements were performed at a temperature of 5 K with a LakeShore TTP4 probing station that enables the application of an in-plane magnetic field of up to 1 T to the sample. IV curves were measured with a Keithley 2635 source meter in a quasistatic mode with a dwell time of 0.1 s on each measurement point.

III. RESULTS

First, we demonstrate ferroelectricity of an ultrathin PTO film, grown on top of a LSMO bottom electrode, using a piezo force microscope (PFM) in dual ac resonance tracking mode [18,19] with an applied ac bias of 100 mV (Fig. 3).

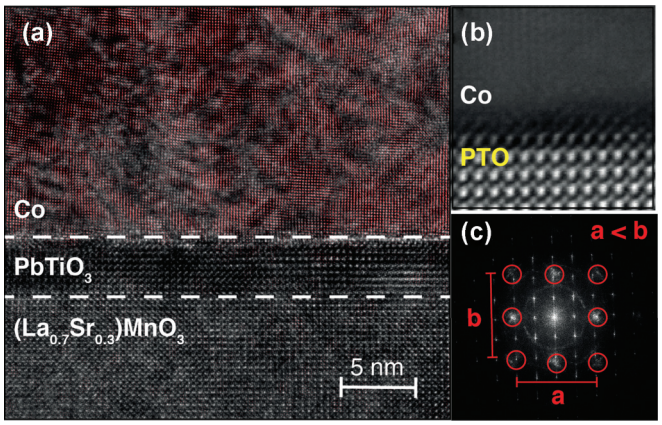

FIG. 2. (Color online) *TEM images of the tunnel junction*. (a) High-resolution electron microscopy image of the heterostructure involving Co/PTO/LSMO. The red areas in the cobalt visualize the regions with the same crystallographic orientation as the PTO. (b) High-angle annular dark field scanning transmission electron microscopy image of the interface between Co and PTO. The atomic columns of cobalt are (barely) visible, showing that Co grows textured on top of epitaxial PTO. (c) Fast Fourier transformation of (a); the spots marked with the red circles can be attributed to the Co with a smaller lattice constant than PTO and LSMO.

As can be seen in Figs. 3(a) and 3(b), both the PFM phase and amplitude of multiple successive loops (phase/amplitude vs applied dc voltage) show hysteresis clear signs of FE switching. The FE remanence was studied by writing a pattern electrically into the film using applied dc biases above the coercivity of ± 3 V. The time between writing and scanning the pattern was several minutes. In Figs. 3(c) and 3(d), one can see the measured PFM response. The good ferroelectric retention of the studied films is evidenced by the 180°-phase contrast [Fig. 3(c)], and evident signal from the ferroelectric domain walls in the corresponding PFM-amplitude image (darker line at the contour of the electrically written domains). The residual contrast observed in the PFM-amplitude image is ascribed to residual ferroelectric imprint as seen in other films [20].

The obtained IV characteristics of the Co/PTO/LSMO tunnel junction for the two opposite polarization directions, measured at a temperature of 5 K, are shown in Fig. 4(a). The current density was fitted by the Brinkman model [21], which delivers parameters for the work functions at the Co (φ_1) and LSMO (φ_2) interfaces, the effective mass m_e, and the thickness d of the tunnel barrier. Short voltage pulses of $+3$ V and -3 V amplitude and 0.5 ms width were applied to fully switch between the ferroelectric polarization states. For the polarization state P_{down}, i.e., pointing towards the LSMO

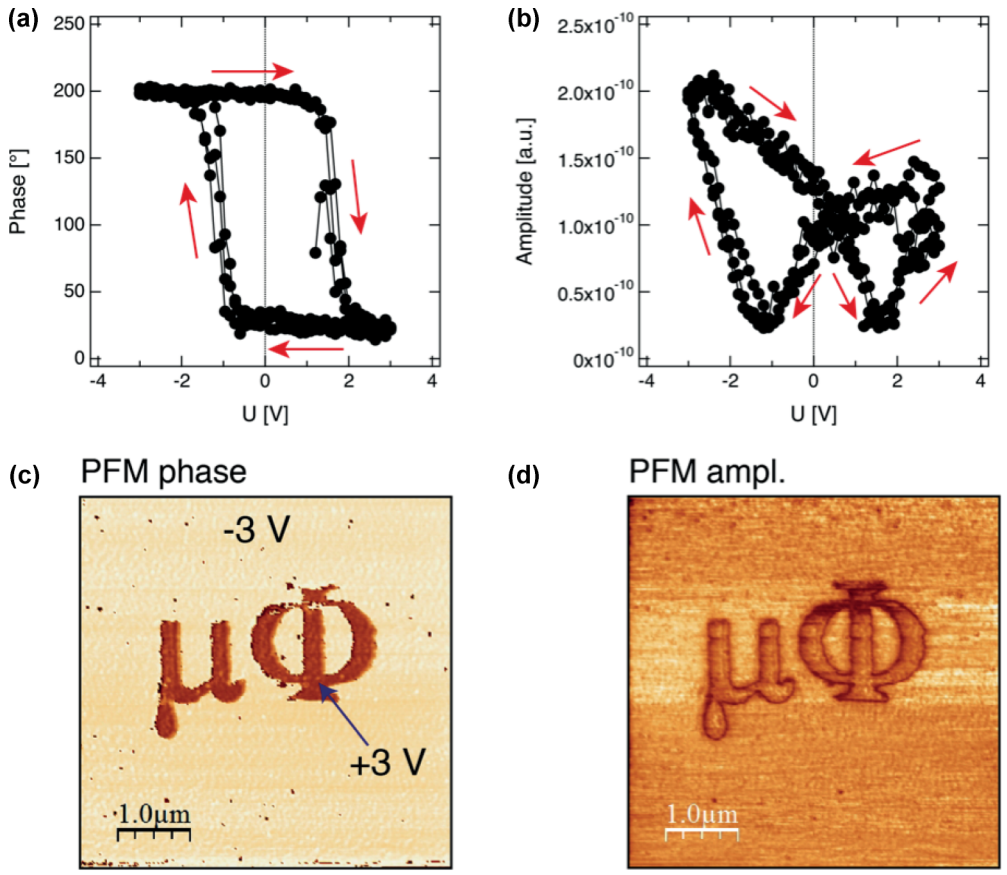

FIG. 3. (Color online) *PFM measurements on an ultrathin PTO(3.2 nm)/LSMO heterostructure*. (a) Multiple loops of the PFM phase versus the applied voltage at fixed tip position. (b) PFM amplitude, simultaneously measured with (a). (c) PFM phase signal picture of a pattern that was written with the c-AFM tip at an applied voltage of ± 3 V; dark corresponds to $-90°$ and bright to $+90°$. (d) Corresponding PFM-amplitude signal (a.u.) of the pattern shown in (c).

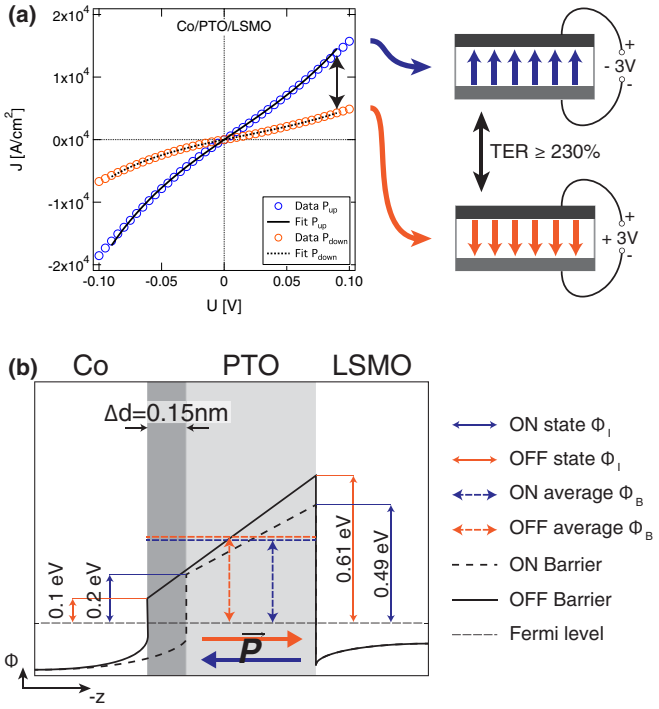

FIG. 4. (Color online) *Band diagram of the tunnel junction with fitting parameters*. (a) Current-voltage characteristics of the measured Co/PTO/LSMO tunnel junction for the two FE polarization states P_{up} (blue) and P_{down} (orange). (b) Schematic of the potential profile across the tunnel junction. The work functions at the interfaces are the fitting parameters of the IV curves (orange for the P_{down} FE polarization state, and blue for the P_{up} one). The dark-gray area visualizes the effective thickness variation.

electrode, the effective resistance is by a factor of 4 larger than that for the opposite polarization P_{up}, i.e., towards the Co electrode.

The resulting fitting parameters (summarized in Table I) were used for the potential profile sketched in Fig. 4(b). Obviously, the gradients of the electric potential inside the ferroelectric do not exhibit the anticipated behavior in correlation to the ferroelectric polarization direction. If the screening lengths of the two electrodes were constant, the electric potential at the cobalt interface would have to be larger for the FE polarization pointing towards LSMO than vice versa (recalling Laplace's equation $\delta\phi = -\rho/\varepsilon_0$). Hence, recalling the dependence of the screening length l from the density of states [DOS; $D(E_F)$] $l \propto [\sqrt{D(E_F)}]^{-1}$, together with the change in screening lengths as a result of the ferroelectric polarization [Fig. 4(b)], the DOS of the electrodes at the interfaces must change accordingly. A reasonable explanation for such a behavior can be a partial metallization of the ferroelectric barrier at the metal interface, which is, in other words, an effective thickness variation of the tunneling barrier. A partial metallization of the FE barrier would naturally lead to a significant change of the DOS at the tunnel barrier interfaces, which could explain the observed behavior.

TABLE I. Fitting parameters as a result from fitting the data in Fig. 1(a) to the Brinkman model.

Polarization	Thickness (nm)	Effective e^- mass	φ_1 (eV)	φ_2 (eV)
Up	3.09	$0.9m_e$	0.20	0.49
Down	3.24	$0.9m_e$	0.10	0.61

Furthermore, the effective thicknesses derived as fitting parameters for the two opposite polarization directions differ by 0.15 nm, whereas the thicker barrier yields the high resistance state. Such a strong change in thickness, however, cannot be accounted for solely by a piezoelectric strain effect induced by the asymmetry of the depolarization fields and their influence on the piezoelectric response of the ferroelectric $PbTiO_3$ alone. The difference of internal fields upon ferroelectric polarization reversal is about $\approx$0.1 V [12] relatively small. The expected piezoelectric effect would lead to a thickness variation in the order of 0.005 nm, more than one order of magnitude smaller than the evaluated effective thickness variation. This value is estimated using a piezoelectric coefficient of $d_{33} = 45 \pm 5$ pm/V [22] measured on a similar, thicker ferroelectic $Pb(Zr_{0.2}Ti_{0.8})O_3$ film. However, to estimate the contribution of a piezo-induced broadening of the tunnel barrier to the TER based on these assumptions, fixed averages of the fitting parameters (see Table I) were used for either polarization direction. A resulting set of IV curves was plotted in Fig. 5(a). The small piezo-induced thickness variation is responsible for a resistance change of just approximately 2%, which is not comparable with the found TER magnitude.

Approaching the significant discrepancy of 3000% between the found thickness variation based on the transport data and the piezoelectric one, *ab initio* studies of the $Co/PbTiO_3/(La_{0.7}Sr_{0.3})MnO_3$ structure were performed. Grown on TiO_2-terminated $SrTiO_3$ [23], $(La_{0.7}Sr_{0.3})MnO_3$ possesses MnO_2 termination towards the FE tunnel barrier. Following the stacking sequence of the ABO_3 perovskite structure, layer-by-layer growth leads to PbO termination of $PbTiO_3$ at the $(La_{0.7}Sr_{0.3})MnO_3$ side and TiO_2 termination at the cobalt interface. Structural relaxation calculations using first-principles methods show that this asymmetry of terminations is responsible for changing the distance between the last Co atom of the top electrode and the last Mn atom of the LSMO bottom electrode by 0.06 nm upon FE polarization reversal. The results show that the thicker barrier corresponds to the polarization direction of PTO towards the LSMO electrode, which is coherent with the findings in Fig. 4. The magnitude of this effect from the *ab initio* calculations already stands in reasonable agreement with the experimentally found thickness variation of 0.15 nm.

Detailed investigations of the local density of states additionally reveal a switchable metallization of the last PTO unit cells next to the cobalt electrode. In Fig. 6, the local density of states of the two unit cells PTO next to the Co electrode along the z axis are presented. The spin-resolved DOS not only show a local spin polarization of the FE tunnel barrier, which would be equivalent to an induced magnetic moment at the titanium cations [24], but also that the extension of electronic states at the Fermi level into the FE strongly varies with the polarization direction. This would mean that, effectively, the tunneling electrons have to overcome a significantly thicker tunnel barrier in the P_{down} case than in the P_{up} case.

Partial metallization of the FE barrier, which is seen near the Co/TiO_2-terminated interface, occurs due to the charge

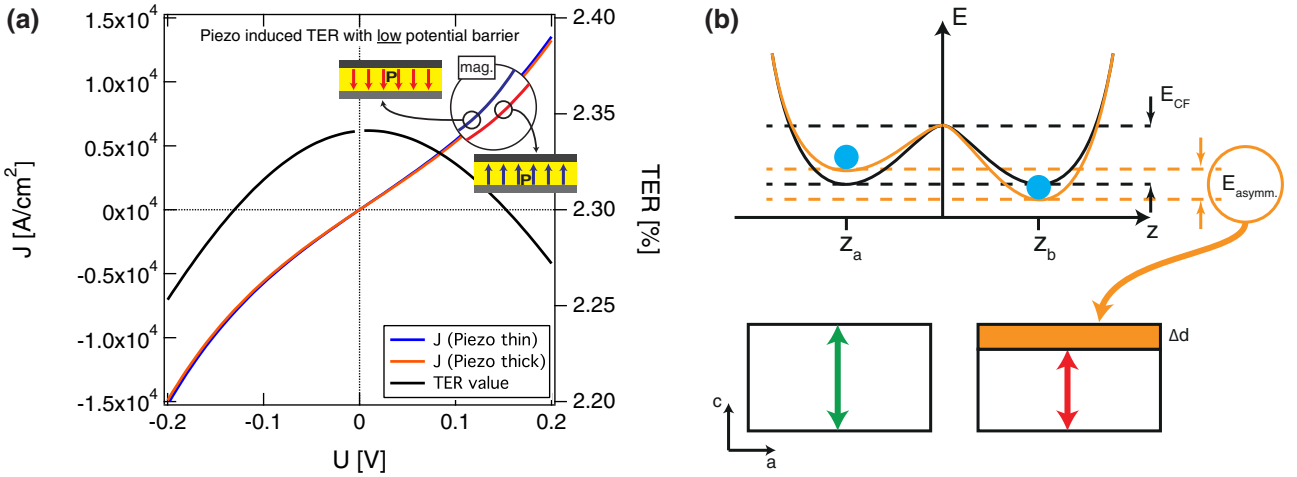

FIG. 5. (Color online) *Influence of piezoelectric thickness variation on the TER.* (a) Calculation of the IV curves, only regarding piezoelectric thickness variation, based on the polarization direction. (b) Sketch of the two ferroelectric states in an E over z (out-of-plane direction) diagram. Due to the (exaggerated) asymmetry caused by different screening lengths and/or terminations at the FE/M interfaces, the stable states are separated by the energy E_{asymm}. This inner electric field causes a piezoelectric deformation Δd, illustrated on the side view of the sample.

transfer between the 3*d* states of the interfacial Co and Ti cations. There is rather strong hybridization between the corresponding 3*d* electronic states and *p* states of intermediate oxygen atoms. As a result, the *n*-type charge carriers, which are localized on the interfacial Ti, appear below the Fermi level in the former band gap of PTO. The computed DOS, shown in Fig. 6, is robustly metallic for the first interfacial TiO_2 layer and marginally metallic for the next PbO layer. When the barrier polarization is directed towards the interface, the separation between the interfacial Ti and Co atoms reduces considerably, which enhances the charge transfer. As a result, the TiO_2 layer of the second PTO unit cell becomes metallic as well. Since the PTO polarization pointing towards Co (P_{up}) is not energetically favorable compared to the polarization P_{down}, the chemical potential of the P_{up} state is placed closer to the conduction band. The charge transfer mechanism was discussed previously for the Fe/TiO_2-terminated interface [25].

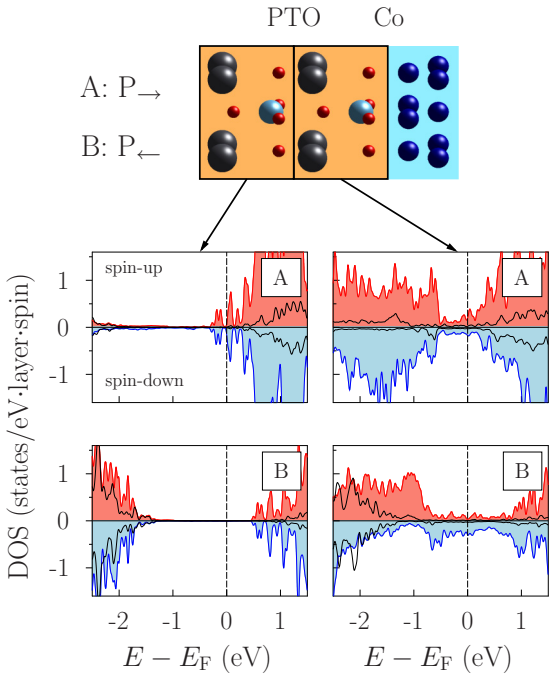

FIG. 6. (Color online) *Calculations of the DOS at the Co/$PbTiO_3$ interface*. The spin-polarized and layer-resolved DOS curves of the first two PTO unit cells at the Co/$PbTiO_3$ interface are plotted by shaded areas and black lines for the TiO_2 and PbO layers, respectively. For the polarization pointing towards the interface, only half of the second PTO unit cell (the TiO_2 layer) is metallic, as shown in the left top DOS panel. The ferroelectric polarization switches the electronic state of the second unit cell from the interface from metallic (A, P_{up}) to insulating (B, P_{down}). Additionally, the distance from Mn to Co changes by up to 0.06 nm, from 2.29 nm (A) to 2.35 nm (B).

In the context of partial metallization of the barrier, a crucial factor of any model is the band gap value, which is systematically underestimated in density functional theory calculations. To explore how the PTO band gap affects its metallization, we used the Hubbard parametrization of electronic correlations on the Ti *d* states, within the GGA + *U* scheme [26]. This allows one to increase the computed band gap of PTO from 1.7 eV at $U = 0$ to 2.4 eV for $U = 4$ eV. However, for the studied tunnel junction, the use of $U = 4$ eV does not change qualitatively the partial metallicity of the PTO barrier, although certain weakening of this effect was obtained. Therefore, one can argue that the electronically driven metallicity at the Co/PTO interface is a robust scenario, which should contribute to the effective thickness variations.

In summary, we have shown that the TER effect of Co/PTO/LSMO tunnel junctions cannot solely be ascribed to the asymmetric screening lengths of the confining electrodes. In contrast, the presented data and theoretical analysis demonstrate that the sign and magnitude of the found TER can be explained by an effective thickness variation upon polarization reversal. This thickness variation is a mixture of structural influences based on the asymmetric termination, and metallization of Co/PTO interface in the studied Co/PTO/LSMO junction, the latter being the main mechanism of the found

TER effect. Note that, despite the good agreement between experiments and theory, the metallization mechanism cannot be completely discriminated from the presence of a depletion region of carriers at the Co/PTO interface that changes its width upon polarization switching, as recently evidenced in similar systems [27]. The evidence of tunnel thickness variation by the application of an electric field deserves further study making use of other materials in which the found effect could be enhanced.

IV. DETAILS OF *AB INITIO* CALCULATIONS

Electronic ground-state properties of the $Co/PbTiO_3/(La_{0.7}Sr_{0.3})MnO_3$ system were modeled using the plane-wave pseudopotential method of both QUANTUM ESPRESSO [28] and VASP [29–31] within the generalized-gradient approximation (GGA) [32]. The supercell that represents this oxide heterostructure consists of five unit cells (u.c.) of the ferroelectric $PbTiO_3$ layer sandwiched between three u.c. of LSMO and five monolayers of cobalt. Both electrodes are ferromagnetic with a parallel orientation of both magnetizations. The in-plane lattice constant was fixed to the bulk value of PTO ($a = 3.892$ Å). In the chosen configuration, the PTO/LSMO interface has the PbO/MnO_2 termination, while the PTO barrier near the cobalt side is terminated by the TiO_2 plane. The LSMO part was simulated using two different structural models. First, the digital alloy model was used where 33% Sr doping creates a continuous SrO layer in LSMO. Secondly, a supercell with larger in-plane dimensions was constructed to simulate the 33% fraction of Sr cations in each oxide layer (perpendicular to the growth direction). The results of both models were compared with respect to the interlayer distances near the PTO/LSMO interface. In the PTO part, the ionic displacements before relaxation were fixed to the corresponding bulk values (0.045 and 0.033 nm in PbO and TiO_2 planes, respectively) according to the polarization direction. The cobalt film was assumed to grow epitaxially on top of the PTO barrier, so that the interfacial cobalt atoms are placed exactly above the oxygen ions of the last PTO layer (see Fig. 6). Finally, a vacuum slice of more than 1.2 nm thickness was added to the system in order to exclude spurious interactions between the periodic images of the supercell along the [001] direction.

Starting from this initial structure, atomic relaxation calculation was performed using VASP [29–31] with the energy cutoff of 460 eV for the representation of the electronic wave functions and the Γ-centered $8\times8\times2$ k-point Monkhorst-Pack mesh [33]. The three central unit cells of PTO were fixed and all other atoms were allowed to move along the [001] direction of the supercell. The threshold for the ionic forces was set to 10^{-2} eV/A. In the relaxed structure, the vacuum layer was removed and a double cell was constructed by creating a mirror image of the whole supercell along the [001] direction and attaching it to the original system. In the resulting supercell (not presented here), the polarization vectors of the two PTO barriers are oppositely oriented, which compensates the dipole moment in the system. The spin-resolved density of states was calculated for this structure using QUANTUM ESPRESSO [28] and the Γ-centered $15\times15\times1$ k-point mesh.

ACKNOWLEDGMENTS

This work was supported in part by the German Research Foundation (DFG) via SFB 762. I.F. acknowledges the Beatriu de Pinós postdoctoral scholarship (2011 BP-A00220 and 2011 BP-A_2 00014) from the Catalan Agency for Management of University and Research Grants (AGAUR-Generalitat de Catalunya).

[1] A. Gruverman, D. Wu, H. Lu, Y. Wang, H. W. Jang, C. M. Folkman, M. Y. Zhuravlev, D. Felker, M. Rzchowski, C.-B. Eom, and E. Y. Tsymbal, Nano Lett. **9**, 3539 (2009).
[2] V. Garcia, S. Fusil, K. Bouzehouane, S. Enouz-Vedrenne, N. D. Mathur, A. Barthélémy, and M. Bibes, Nature (London) **460**, 81 (2009).
[3] A. Chanthbouala, V. Garcia, R. O. Cherifi, K. Bouzehouane, S. Fusil, X. Moya, S. Xavier, H. Yamada, C. Deranlot, N. D. Mathur, M. Bibes, A. Barthélémy, and J. Grollier, Nat. Mater. **11**, 860 (2012).
[4] D. J. Kim, H. Lu, S. Ryu, C.-W. Bark, C.-B. Eom, E. Y. Tsymbal, and A. Gruverman, Nano Lett. **12**, 5697 (2012).
[5] A. Quindeau, D. Hesse, and M. Alexe, Front. Phys. **2**, 7 (2014).
[6] M. Y. Zhuravlev, R. F. Sabirianov, S. S. Jaswal, and E. Y. Tsymbal, Phys. Rev. Lett. **94**, 246802 (2005).
[7] H. Kohlstedt, N. A. Pertsev, J. Rodríguez Contreras, and R. Waser, Phys. Rev. B **72**, 125341 (2005).
[8] E.Y. Tsymbal and H. Kohlstedt, Science **313**, 181 (2006).
[9] M. Gajek, M. Bibes, S. Fusil, K. Bouzehouane, J. Fontcuberta, A. Barthélémy, and A. Fert, Nat. Mater. **6**, 296 (2007).
[10] Z. Wen, C. Li, D. Wu, A. Li, and N. Ming, Nat. Mater. **12**, 617 (2013).
[11] Y. W. Yin, J. D. Burton, Y.-M. Kim, A. Y. Borisevich, S. J. Pennycook, S. M. Yang, T. W. Noh, A. Gruverman, X. G. Li, E. Y. Tsymbal, and Q. Li, Nat. Mater. **12**, 397 (2013).
[12] Y. Liu, X. Lou, M. Bibes, and B. Dkhil, Phys. Rev. B **88**, 024106 (2013).
[13] H. J. Mao, P. X. Miao, J. Z. Cong, C. Song, B. Cui, J. J. Peng, F. Li, G. Y. Wang, Y. G. Zhao, Y. Sun, L. R. Xiao, and F. Pan, J. Appl. Phys. **116**, 053703 (2014).
[14] L. Jiang, W. S. Choi, H. Jeen, S. Dong, Y. Kim, M.-G. Han, Y. Zhu, S. V. Kalinin, E. Dagotto, T. Egami, and H. N. Lee, Nano Lett. **13**, 5837 (2013).
[15] N. García, Appl. Phys. Lett. **77**, 1351 (2000).
[16] J. Ventura, J. M. Teixeira, J. P. Araujo, J. B. Sousa, P. Wisniowski, and P. P. Freitas, Phys. Rev. B **78**, 024403 (2008).
[17] D. Pantel and M. Alexe, Phys. Rev. B **82**, 134105 (2010).
[18] B. J. Rodriguez, C. Callahan, S. V. Kalinin, and R. Proksch, Nanotechnology **18**, 475504 (2007).
[19] B. J. Rodriguez, S. Jesse, K. Seal, N. Balke, S. V. Kalinin, and R. Proksch, in *Scanning Probe Microscopy of Functional Materials*, edited by S. V. Kalinin and A. Gruverman (Springer, New York, 2011), Chap. 17.

[20] M. Gich, I. Fina, A. Morelli, F. Sanchez, M. Alexe, J. Gazquez, J. Fontcuberta, and A. Roig, Adv. Mater. **26**, 4645 (2014).
[21] W. F. Brinkman, J. Appl. Phys. **41**, 1915 (1970).
[22] I. Vrejoiu, G. Le Rhun, L. Pintilie, D. Hesse, M. Alexe, and U. Gösele, Adv. Mater. **18**, 1657 (2006).
[23] G. Koster, B. L. Kropman, G. J. H. M. Rijnders, D. H. A. Blank, and H. Rogalla, Appl. Phys. Lett. **73**, 2920 (1998).
[24] V. S. Borisov, S. Ostanin, I. V. Maznichenko, A. Ernst, and I. Mertig, Phys. Rev. B **89**, 054436 (2014).
[25] M. Fechner, I. V. Maznichenko, S. Ostanin, A. Ernst, J. Henk, P. Bruno, and I. Mertig, Phys. Rev. B **78**, 212406 (2008).
[26] V. I. Anisimov, F. Aryasetiawan, and A. I. Lichtenstein, J. Phys.: Condens. Matter **9**, 767 (1997).
[27] G. Radaelli, D. Gutiérrez, F. Sánchez, R. Bertacco, M. Stengel, and J. Fontcuberta, Adv. Mater. **27**, 2602 (2015).
[28] P. Giannozzi, S. Baroni, N. Bonini, M. Calandra, R. Car, C. Cavazzoni, D. Ceresoli, G. L. Chiarotti, M. Cococcioni, I. Dabo, A. Dal Corso, S. de Gironcoli, S. Fabris, G. Fratesi, R. Gebauer, U. Gerstmann, C. Gougoussis, A. Kokalj, M. Lazzeri, L. Martin-Samos *et al.*, J. Phys.: Condens. Matter **21**, 395502 (2009).
[29] G. Kresse and J. Hafner, Phys. Rev. B **49**, 14251 (1994).
[30] G. Kresse and J. Furthmüller, Phys. Rev. B **54**, 11169 (1996).
[31] J. Hafner, J. Comput. Chem. **29**, 2044 (2008).
[32] J. P. Perdew, K. Burke, and M. Ernzerhof, Phys. Rev. Lett. **77**, 3865 (1996).
[33] H. J. Monkhorst and J. D. Pack, Phys. Rev. B **13**, 5188 (1976).